SUPPORTING INFORMATION FOR

Multiproxy evidence for leaf browsing and closed habitats in extinct proboscideans (Mammalia, Proboscidea) from Central Chile

Erwin González-Guarda, Alia Petermann-Pichincura, Carlos Tornero, Laura Domingo, Jordi Agustí, Mario Pino, Ana M. Abarzúa, José M. Capriles, Natalia Villavicencio, Rafael Labarca, Violeta Tolorza, Paloma Sevilla, Florent Rivals

Corresponding author. Email: erwingonzalezguarda@gmail.com

Geographic setting, climate and vegetation of the study area

From the late Miocene onwards, the vegetation of the study area (Fig. S1) began to be determined by the effect of the so-called Arid Diagonal. During the Quaternary, due to the extent geographical isolation of this region and the damping effect of the Pacific Ocean on the temperature of the western margin of the continent, particularly at middle latitudes in the Coastal Range of Chile, this region was a key refuge for biota during glaciations. Radiocarbon dating of the fossil record on gomphotheres from Chile, only encompasses a chronological range between ~30,000–12,000 cal yr BP (Fig. S2). In this time range, the climate was colder and wetter than today. During the Last Glacial Maximum (LGM, 26,500–19,000 cal yr BP; at a global level) precipitations were double and summer temperatures were 6º–8º C colder than today (1). One of the most striking aspects of the late Pleistocene was the high humidity recorded at latitudes between 31º–36º S (Fig. S1), which favored the expansion of vast forested areas. Between 38º–42ºS, glaciers occupied the Andean range and

www.pnas.org/cgi/doi/10.1073/pnas.1804642115

part of the Central Depression between 33,600–19,000 cal yr BP (2), deeply affecting the vegetation assemblage. However, the oceanic influence along with the physical heterogeneity of the landscape provided a mosaic of habitats for forest refugia during this glacial period (3). An increase in temperatures about ~18,000 cal yr BP (Last Glacial Termination) triggered the onset of the deglaciation (4), but the climate continued to be colder and wetter than today. North Patagonian temperate rainforests were fully established after the glacial retreat (2). By ~16,800 cal yr BP, temperatures approached average interglacial values, albeit with cold reversions between ~14,700 and 11,500 cal yr BP, as documented in northwestern Patagonia (2). During the early Holocene (~11,700–9,000 cal yr BP), between 31º–34ºS, a process of abrupt climatic change has been detected by the pollen records recovered from continental sites, which suggest the presence of large areas of grassland and regional conditions becoming drier and warmer (5). A similar trend was noted when estimating sea surface temperatures (6). Between 38º–42º S, a drier and warmer phase was also recorded by sea surface temperatures (from alkenones) (4), and the most thermophilic taxa of the Valdivian forest (as evidenced by the palynological record) began to dominate from ~11,000 cal yr BP (2).

Preservation of the isotopic signal

The samples analyzed in this study show an average $\Delta^{18}O_{CO3-PO4}$ value of ~9.0‰. This value is within the established $\Delta^{18}O_{CO3-PO4}$ range for unaltered biopatite of present-day mammals (i.e., 8.6 – 9.1‰) (7), pointing to the preservation of original $\delta^{18}O_{CO3}$ and $\delta^{18}O_{PO4}$ values. The correlation coefficient between these values is high ($R = 0.9$, $p < 0.001$), which suggests that the CO_3^{-2} and PO_4^{-3} in bioapatite are cogenetic equilibrium precipitates from body water at relatively invariant mammalian body temperatures. Carbon:nitrogen (C:N) ratios of the selected fossil material are within the accepted range for modern collagen (2.9 and 3.6 in living mammals) (8) supporting the preservation of the original $\delta^{13}C$ and $\delta^{15}N$ biogenic signal. Some samples had a value slightly below 2.9, however, we included them in the analysis since they had percentages of C_{coll} and N_{coll} higher than the accepted 13% and 4.8% values for unaltered collagen, respectively (9).

Results

Stable Isotopes Analysis

The Mann-Whitney U test shows significant differences between NC and SC gomphotheres in terms of both $\delta^{13}C_{bio}$ and $\delta^{18}O_{bio}$ values (Table S1). Regarding the NC area, gomphothere $\delta^{13}C_{bio}$ values point to the existence of a closed-canopy forest (3% of samples) and woodland-mesic C_3 grassland (84% of samples), open woodland-xeric C_3 grassland (8% samples), and mixed C_3–C_4 grassland (5% of samples) (Fig. 2). As far as the SC area is concerned, gomphothere $\delta^{13}C_{bio}$ values point to the presence of a closed-canopy forest (13% of samples), and woodland-mesic C_3 grassland (87% of samples) (Fig. 2). Figure A shows the $\delta^{13}C_{bio}$ (‰, VPDB) and $\delta^{18}O_{CO3}$ (‰, VSMOW) values. The Mann-Whitney U test shows significant differences between NC and SC gomphotheres in terms of both $\delta^{13}C_{coll}$ and $\delta^{15}N$ values (Figure 4B; Table S1), with NC depicting higher values. The Mann-Whitney U test reveals a significant difference between NC and SC gomphotheres in terms of the estimated dietary modern equivalent (i.e., vegetation) carbon stable isotope value ($\delta^{13}C_{diet,meq}$) (Table S2), with NC showing a higher $\delta^{13}C_{diet,meq}$ value. The Mann-Whitney U test also shows a significant difference between NC and SC in terms of mean annual temperature values (Table S3), with the NC area recording a higher temperature.

Dental Microwear Analysis

Figure S3 shows photomicrographs of gomphothere tooth enamel, which generally display high percentages of coarse and hyper-coarse scratches and low numbers of pits and fine scratches. The raw data are presented in Table S5, whereas a summary of dental microwear results is presented in Table S6. The average values for the numbers of pits and scratches show a large range of variation in gomphotheres. When compared to known values of the average number of pits versus the average number of scratches per taxon for extant ungulates (10), it is observed that our results do no fall in the 95% confidence ellipse of the extant leaf browsers (Fig. 3A). However, while the mean does not fall within the typical range of modern leaf browsers, values recorded are closer to this type of diet. The SWS (scratch width score = 1.7) from NC falls slightly within a grazing dietary behavior and within a fruit browsing diet. The SWS (2.0) from SC falls inside the fruit browsing diet (10). However, the high percentages of hyper-coarse suggest a browsing behavior (e.g., bark or branches of plants) (10). Morever, when analyzing the percentage of individuals with low numbers of scratches (%0–17), the diet of the gomphotheres of the two areas analyzed here correspond to a leaf browsing diet (Table S5). Since this last calculation is more conclusive to delimit a grazing or browsing behavior (11), the results point to a leaf browsing diet in both areas.

Analysis of Microfossils from Dental Calculus

All analyzed samples show the presence of phytoliths. Additionally, ancient starch and other siliceous particles like sponge spicules and diatoms were also present. Most of the samples (i.e., 88%) show a predominance of tree and shrub elements (Table S6). Morphotypes such as polygonal, polyhedral, spherical or vascular tissue (Fig. 3B) support a diet based on trees and shrubs (Fig. S4). More specifically, the tracheids observed in samples LP13, LP14, TR1 and SGOPV47h, are a diagnostic character of conifers. The simultaneous presence of phytoliths from trees/shrubs and the Poaceae/Cyperaceae families shows a mixed consumption of woody plants and herbs. Grass phytoliths found in the samples include short cells identified as belonging to the Pooideae and Bambusoideae subfamilies (*Chusquea sp*.). A high quantity of secondary elements like sponge spicules and diatoms (Table S6) is likely indicative of a fortuitous ingestion in wetland environments (12).

Materials and Methods

Materials

A multi-proxy approach involving Stable Isotope Analysis (SIA), Dental Microwear Analysis (DMA) and Analysis of Microfossils from Dental Calculus

(AMDC) was carried out on 79 teeth of the gomphothere *Notiomastodon platensis*.

SIA. The measurements obtained from this analysis provide information about dietary resources and trophic level of the analyzed specimens, and also features related to environmental and climatic variability. Stable isotope analyses carried out on tooth enamel and collagen in dentine samples mainly record the early stages of a mammal’s life, whereas stable isotope analyses performed on bone collagen reflect a mammal’s lifetime average or even the last stages of the animal´s life (8).

DMA. This is a method that provides an insight, through the study of tooth enamel surfaces, into the dietary patterns of a mammal over the last days or weeks before its death. Dental microwear provides a glimpse into available vegetation and habitat, as well as short-term dietary traits (11, 13).

AMDC. Plants micro remains attached in dental calculus can provide direct information on feeding habits (14) and a long-term dietary signal (15). The accurate timespan involved in dental calculus is not yet clarified, as the formation processes and its composition can be highly variable among and within individuals (16). For this reason, it is not possible to determine when, within the lifetime of an animal, a specific plant micro remain was ingested (17). Considering that older individuals present more microremains (16), dental calculus can to represent a mean of multiple feeding events in the animal’s life, assuming there is no replacement or removal of calculus deposits.

15 teeth were analyzed by all three analytical proxies; 29 teeth were analyzed by two (DMA and AMDC) and 35 teeth were analyzed only by SIA (Dataset).

Samples selected for this study come from 30 sites located at latitudes between

31ºS and 36ºS (North–Central = NC; Mediterranean climate), and between 38ºS and 42ºS (South–Central = SC; Temperate climate) (Fig. 1; Dataset). The chronology of the selected specimens spans a time range from ~ 30,000–12,000 cal yr BP, bracketing the Pleistocene-Holocene transition. The whole dataset of selected samples with their respective analyses is listed in Dataset. The multi-proxy analysis was not possible in all teeth, as some of them presented evident taphonomic and diagenetical alterations (Dataset). In order to avoid the influence of mother´s milk on the isotopic signal, we selected mostly teeth that developed during adulthood (i.e. M2/m2; M3/m3) (Dataset).

Methods

SIA. A rotary hand drill with a diamond-tipped dental burr was used to recover enamel from an area of the tooth as large as possible to avoid seasonal bias at the time of mineralization. Five to six milligrams of tooth enamel were sampled for bioapatite $\delta^{13}C$ and $\delta^{18}O$ analyses, whereas around 50–100 mg of bone chips were collected for collagen $\delta^{13}C$ and $\delta^{15}N$ analyses. Stable isotope results are reported in the δ-notation $\delta^{H}X_{sample}=[(R_{sample}-R_{standard})/R_{standard}]x1000$, where X is the element, H is the mass of the rare, heavy isotope, and $R={}^{13}C/{}^{12}C$, ${}^{18}O/{}^{16}O$ or ${}^{15}N/{}^{14}N$. $\delta^{13}C$ and $\delta^{18}O$ values are expressed in the Vienna-Pee Dee Belemnite (VPDB) standard, although $\delta^{18}O$ values are also given in terms of the VSMOW (Vienna Standard Mean Ocean Water) standard, so that VPDB values can be converted into VSMOW applying the following formula: $\delta^{18}O_{SMOW} = (1.0309 \times \delta^{18}O_{VPDB}) + 30.909$. $\delta^{15}N$ values are given relative to atmospheric nitrogen (AIR).

Bioapatite $\delta^{13}C$ and $\delta^{18}O$ values were measured at the *Service de Spectrométrie de Masse Isotopique du Muséum National Histoire Naturelle (*SSMIM-MNHN) in Paris, (France). There samples were treated following procedures described in Tornero et al. (18). Dry samples weighing ~600 micrograms were introduced into a Kiel IV device interfaced to a Delta V Advantage isotope ratio mass spectrometer (IRMS). All samples were measured in two different analytical series. The accuracy and precision of the measurements were checked using an internal laboratory calcium carbonate standard (Marbre LM normalized to NBS 19). During the analysis period a total of 16 Marbre LM samples gave a mean $\delta^{13}C$ value of +2.09±0.037‰ (1σ) (expected value +2.13‰) and a $\delta^{18}O$ value of -1.92 ± 0.071‰ (1σ) (expected value -1.83‰). Bioapatite $\delta^{13}C$ and $\delta^{18}O$ values from SC gomphotheres were taken from González-Guarda et al. (19) and they were analysed at the Stable Isotope Laboratory of the University of California Santa Cruz (USA)

Collagen extractions were performed at the Biomolecular laboratory of the Institute of Human Palaeoecology and Social Evolution (Tarragona, Spain). Collagen extraction followed original protocols proposed by Longin (20) and modified by Bocherens et al. (21). Bones fragments were cleaned mechanically to remove the surface while shards of bones (ca. 300 to 350 mg) were demineralized using 1 M HCl, rinsed with distilled water and gelatinized with 0.002 M HCl at 100°C for 17 h. Samples were then filtered, frozen and freeze dried at the ICIQ (Institute of Chemical Research in Catalonia). Collagen samples weighting about 0.3 mg were analyzed in duplicate using a Thermo Flash 1112 elemental analyzer (EA) coupled to a Thermo Delta V Advantage isotope ratio mass spectrometer (IRMS) with a Conflo III interface, at the

Institute of Environmental Science and Technology, Autonomous University of Barcelona. The international laboratory standard IAEA 600 (caffeine) was used as a control. The average analytical error was <0.2‰ (1σ) as determined from the duplicate analyses of $\delta^{13}C$ and $\delta^{15}N$. The standard used for $\delta^{13}C$ was Vienna PeeDee Belemnite (VPDB), and the standard for $\delta^{15}N$ was air N_2 (AIR). Collagen $\delta^{13}C$ and $\delta^{15}N$ values from SC gomphotheres were taken from González-Guarda et al. (19) and they were analysed at the Stable Isotope Laboratory of the University of California Santa Cruz (USA).

In this study, we consider a $\delta^{13}C_{atmCO2}$ value of -6.5‰, accepted for the late Pleistocene (22). Therefore, the ranges that we considered to classify vegetation according to $\delta^{13}C_{enamel}$ values, after correction for trophic discrimination (23), are: 1) closed-canopy forest, -20.5 to -14.5‰; 2) woodland-mesic C_3 grassland, -14.5 to -9.5‰; 3) open woodland-xeric C_3 grassland, -9.5 to -6.5‰; 4) mixed C_3–C_4 grassland, -6.5‰ to -1.5‰; and 5) pure C_4 grassland, -1.5‰ to +6.5‰ (24).

To calculate Mean Annual Temperatures (MATs), we first estimated the $\delta^{18}O_{mw}$ value ingested by gomphotheres using their enamel $\delta^{18}O_{PO4}$ values and then applied the $\delta^{18}O_{mw}$-$\delta^{18}O_{PO4}$ linear regression established for their nearest-living relatives: modern elephants. Such equation was selected assuming that there are no significant differences in the fractionation factor between $\delta^{18}O_{PO4}$ and $\delta^{18}O_{mw}$ of extinct gomphotheres and extant elephants. The equation used was the following: $\delta^{18}O_{mw\ (VSMOW)} = (\delta^{18}O_{PO4\ (VSMOW)} - 23.3)/0.94$ (25). To calculate the MAT, a linear equation between the MAT and $\delta^{18}O_{mw}$ values was used: MAT (ºC) = $\delta^{18}O_{mw}$ (VSMOW) +12.68)/0.36 ($R^2 = 0.72$) (26). This equation was chosen because it uses data from all meteorological stations around the world;

therefore, all existing climate regimes are represented within it. From bioapatite $\delta^{13}C$ values, modern equivalent vegetation was calculated using the following equation: $\delta^{13}C_{vegetation} = \delta^{13}C_{leaf} + (\delta^{13}C_{modernatmCO2} - \delta^{13}C_{ancientatmCO2})$, where $\delta^{13}C_{leaf} = \delta^{13}C_{tooth}$ -14.1‰ (23), $\delta^{13}C_{modernatmCO2}$ is -8‰ and $\delta^{13}C_{ancientatmCO2}$ is -6.5‰ (late Pleistocene) (22). Mean Annual Precipitation (MAP) was calculated using the following equation: $\delta^{13}C$ (‰, V-PDB) = -10.29 + 1.90 x 10^{-4} Altitude (m) - 5.61 $\log_{10}$ (MAP + 300; mm/yr) - 0.0124 Abs (latitude, º) (27).
A non-parametric Mann-Whitney U test was used to compare isotopic values of the gomphotheres from NC and SC. The significance level was set at $p = 0.05$. $\delta^{13}C$ will be expressed as follows: $\delta^{13}C_{bio}$ for bioapatite samples, and $\delta^{13}C_{coll}$ for bulk-collagen samples.

DMA. For this study we had access to almost all the gomphothere molars registered in Chile. Nevertheless, only 35 samples could be studied as they did not show evidences of extensive taphonomic and diagenetical alteration (Dataset). Second upper and lower molars (M2 and m2, respectively), were preferentially selected, although first (M1/m1) and third (M3/m3) molars were as well studied in order to expand the dataset (Dataset). Most of the samples showed an intermediate wear stage (28). The microwear analysis followed the methodology specified by Asevedo et al. (28): the selection of the occlusal enamel area of the metaloph/metalophid on both the postrite and pretrite cusps. The dental microwear features were analyzed using a light stereomicroscope and 35 x magnification. The cleansing, molding, casting, and examination regime was developed following to Solounias and Semprebon (10). The microwear pattern was analyzed on the occlusal area of dental enamel, and we observed and quantified the following features: i) the average number of pits (rounded features) versus average number of scratches (elongated features) per taxon were assessed within a 0.16 mm^2 area (ocular reticle); ii) scratch textures were qualitatively scored as being either predominantly fine, predominantly coarse, or a mixture of fine and coarse types of textures per tooth surface following the criteria described in Solounias and Semprebon (10) to recognize these textures; iii) a scratch width score (SWS) was obtained by giving a score of 0 to teeth with predominantly fine scratches per tooth surface, 1 to those with a mixture of fine and coarse types of textures, 2 to those with predominantly coarse scratches and 3 to those with predominantly hyper-coarse scratches per tooth surface. Individual scores for a sample were then averaged to get the average scratch width score for that taxon (29); and iv) the leaf browsers, grazers, and mixed feeders show distinctive patterns when the percentage of raw scratches in a sample that fall into a low raw scratch range are calculated (i.e., percentage of scratches that fall between 0–17). On the one hand, there is no overlap between the low-scratch ranges of extant leaf-dominated browsers and grazers (i.e., 72.73–100% of extant leaf-dominated browsing taxa have average numbers of individual scratches that fall between 0–17 and 0–22.2% of extant grazing taxa have average numbers of individual scratches that fall between 0–17). On the other hand, no overlap is seen in the ranges of browsers and seasonal or regional mixed feeders (20.93–70% of taxa have average numbers of individual scratches that fall between 0–17) and the overlap between grazers and the latter it is not significant. Fruit-dominated browsers as a group exhibit a very wide range of scratch widths (0–86% of scratches fall between 0–17) perhaps reflecting differences in fruit rinds and seed coats in terms of toughness and/or degree of ripeness of fruits at the time of consumption, which may also explain their broad scratch textural ranges. The degree of large pitting and puncture- like large pits may be used to distinguish fruit browsing (11).

AMDC. For calculus extraction, we performed a dry cleaning to remove coarse sediment and a second cleaning with acetone to remove the adhered sediment. The calculi were removed, using a dental curette to obtain small fragments. This method allowed remove sediment and minimize enamel surface damage.
The extraction of microfossils from the calculus samples was done using the chemical processing method described by Wesolowski et al. (30). To estimate the quantities of microfossils in dental calculus a *Lycopodium* tablet was added to each sample. A 10% solution of hydrochloric acid was added to each sample to dissolve completely the carbonates. After the calculus was dissolved, the tubes were centrifuged at 1000 RPM for 5 min and the supernatant was removed and the sample washed with distilled water and centrifuged again. After the last centrifugation, the distilled water was replaced by 96% ethanol. Three slides were prepared for each of the samples using Entellan ®. The slides were examined under a polarized light microscope with 400x and 630x magnification. All microfossils found including: phytoliths, starch granules, charcoal and *Lycopodium* spores were counted and recorded. To calculate the concentration of microfossils, we applied Maher's (31) method as modified by Wesolowski et al. (32).

Dating. Ten new radiocarbon dates (Table S7) are reported in this study. All of them were obtained from molar root fragments specifically selected to enhance the possibilities of isolating bone collagen. The collagen extracted was broken down into individual amino acids and purified using XAD2 resin following the methods described by Stafford et al. (33). The resultant amino acid solution was combusted and radiocarbon dated using accelerator mass spectrometry (AMS). The samples were prepared and radiocarbon dated at the Human Paleoecology and Isotope Geochemistry Lab of the Pennsylvania State University (PSUAMS), Keck Carbon Cycle AMS Facility (KCCAMS) of the University of California-Irvine, and the Center for Accelerator Mass Spectrometry CAMS in Lawrence Livermore National laboratories, California. All dates have been calibrated to calendar years using Calib 7.02 (34) and the SH-cal13 curve was applied.

Smooth areas located in central Chile. We calculated the Cross Sectional Curvature (CSC) from the SRTM DEM (30 m resolution). The CSC measures the surface curvature orthogonally across slope directions. We identify a threshold value of CSV equal to 0.15 between gentle and steep terrains, and we selected the smooth terrains as those where $|\text{CSC}| \leq 0.15$. The total area lower than 2000 m and with $|\text{CSC}| \leq 0.15$ is 96738.06 km^2.

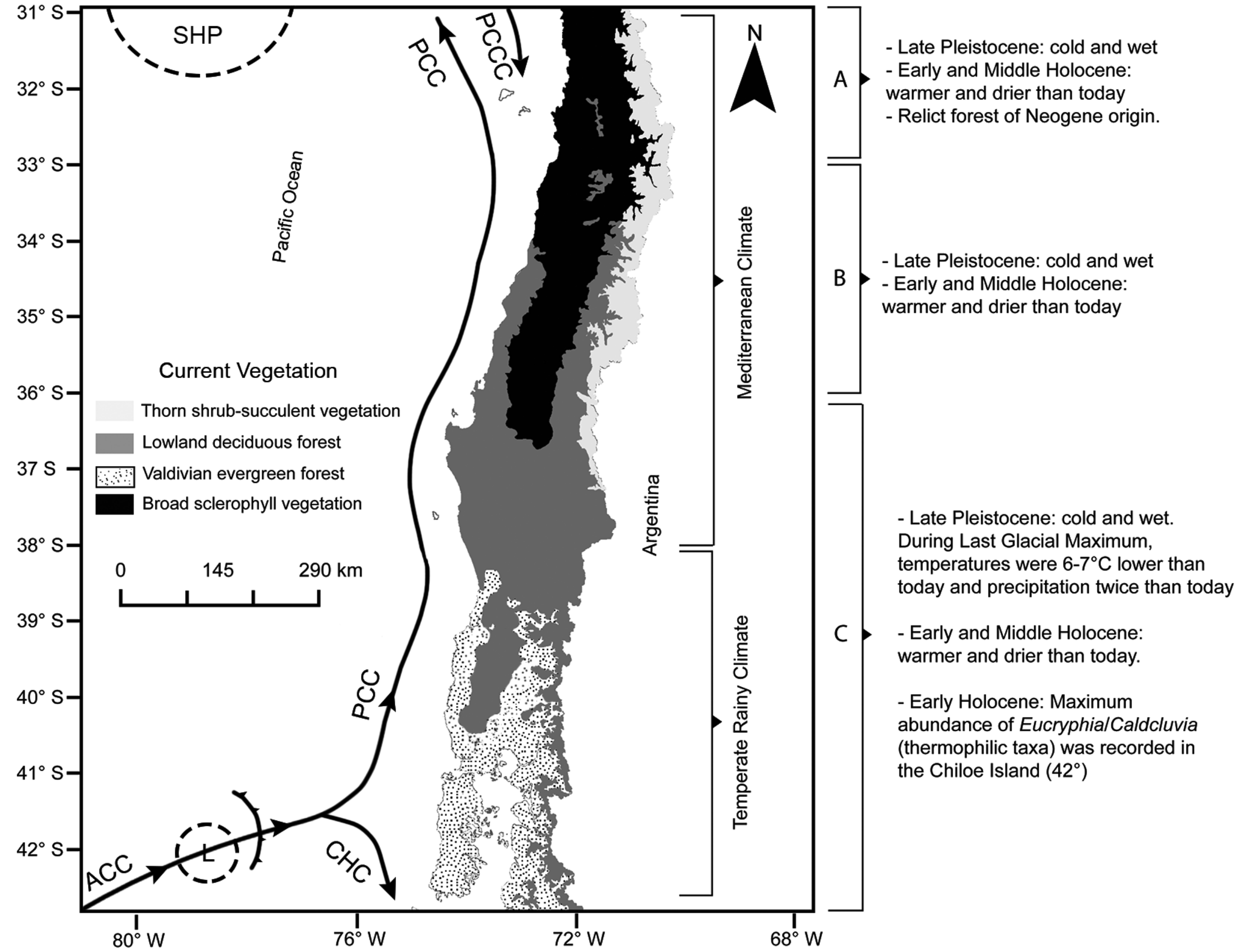

Figure S1. Climatic and vegetational situation of the study area. The vegetation assembly of the study area is determined mainly by the presence of the Andes Range, causing severe rain shadow effect in different areas of the continent, isolating and singularizing the flora and vegetation of the Pacific Ocean edge of South America, with respect to the vegetation existing to the east of the Andes (Arid Diagonal). 31º–38ºS: this area is under the influence of both the southward flowing Peru–Chile Countercurrent (PCCC) and the northward flowing Peru–Chile Current (PCC). The PCC, Subantarctic surface waters originate in the northern region of the Subantarctic Front. At 30º S, the influence of the PCC is greater during austral winter, whereas the influence of the PCCC, bringing relatively warm waters from the low latitudes, is strong in austral summer (6). In austral summer, the very stable SHP cell (subtropical high pressure) located around 30º S blocks the frontal system of the L (low-pressure belt associated with the westerlies) (generating drought; 35) (centered around 49–50ºS). In austral winter, the SHP is shifted northward around 30ºS and the L reaches North Central Chile (6), consequently generating rains (35). 38º–43ºS: this study area is located at the northern margin of the Antarctic Circumpolar Current (ACC) under the influence of subantarctic surface waters and steep latitudinal SST Surface Sea Temperature (SST). The northern part of the ACC splits around 43ºS into the PCC flowing northward and the Cape Horn Current (CHC) turning toward the south. In summer, the storm track activity (associated to the westerlies in the Southern Hemisphere) can be as strong as in winter, but is located slightly equatorward of its winter position, and is concentrated in a tight band centered around 49º–50ºS. In winter, storm track activity extends over a broader range of latitudes and is centered only 2º poleward from its summer position. The strong SST gradients associated with the ACC are marked by a northward latitudinal shift of ~5º in Winter (4).

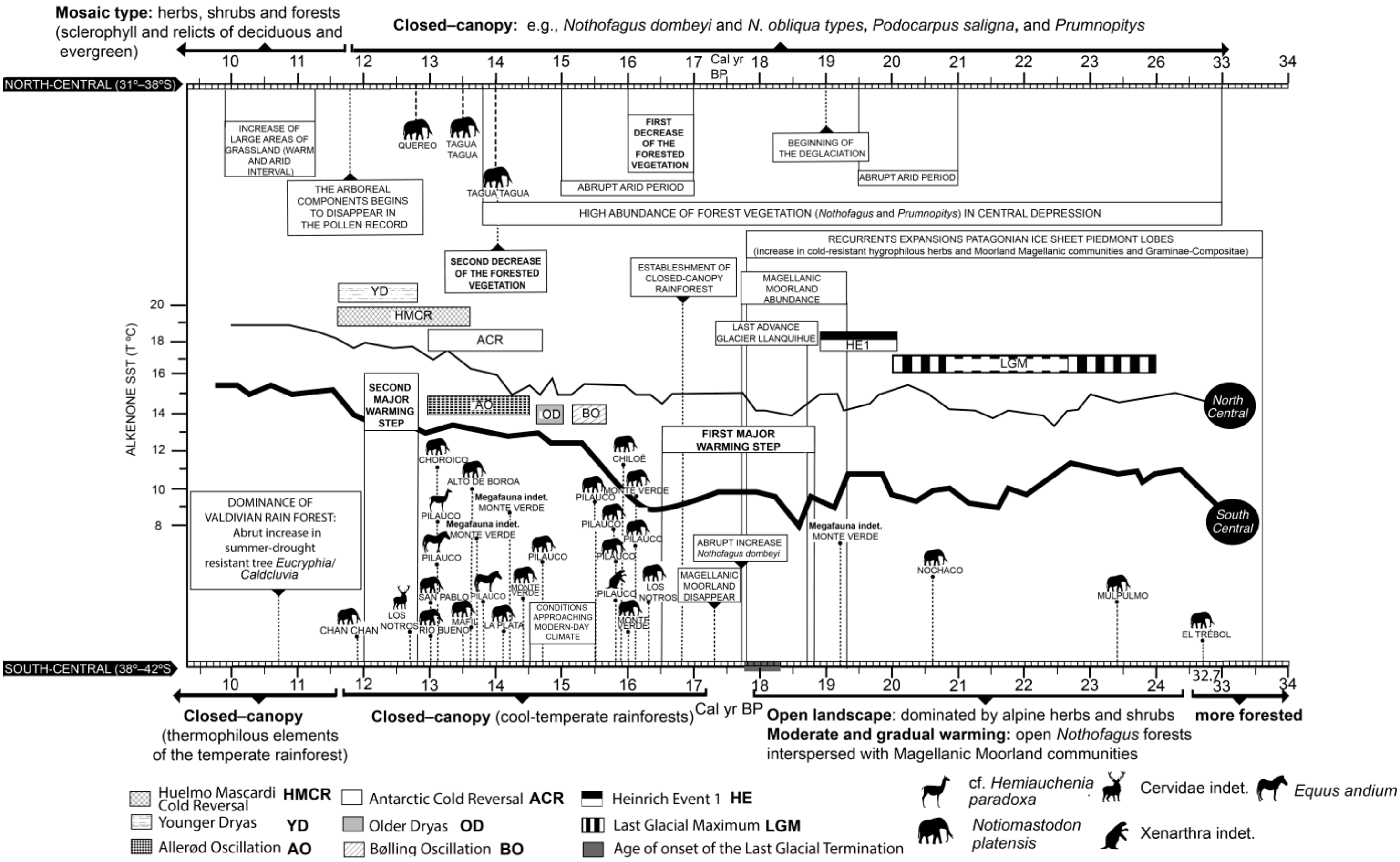

Figure S2. Major climatic events during the Last Glacial Maximum and Last Glacial Termination in Chile. The curve of the North–Central area (thin solid line) depicts a well-dated and high-resolution alkenone-based sea surface temperature (SST) record from sediment core collected about 50 km offshore (30ºS) (6). The curve of the South–Central area (thick solid line) shows a well-dated and high-resolution alkenone-based sea surface temperature (SST) record from sediment core collected at the SE-Pacific of southern Chile (41ºS) (4). Geomorphological and vegetational events (in the Central Depression) come from the literature mentioned in the Dataset. Animal silhouettes represent samples with calibrated radiocarbon dating (mean probability). Radiometric data were taken from González-Guarda et al. (19) and this study. Environmental features: HMCR and YD, expansion of *Podocarpus nubigena* (a cold-resistant shade-tolerant conifer) and wet/dry anomalies in precipitation. AO and BO, abrut expansion of thermophilous, closed canopy NorthPatagonian rainforest. ACR, increase in the number of cold resistant hygrophilous trees and a decline in thermophilic taxa (North Patagonian rainforest). OD, increase of the cold-resistance *Podocarpus nubigena*. HE1: abrupt increase in thermophyllic vegetation assemblages. LGM, increase in cold-resistant hygrophilous herbs and Moorland Magellanic communities. Among 24–33 cal yr BP, the X axis is abbreviated.

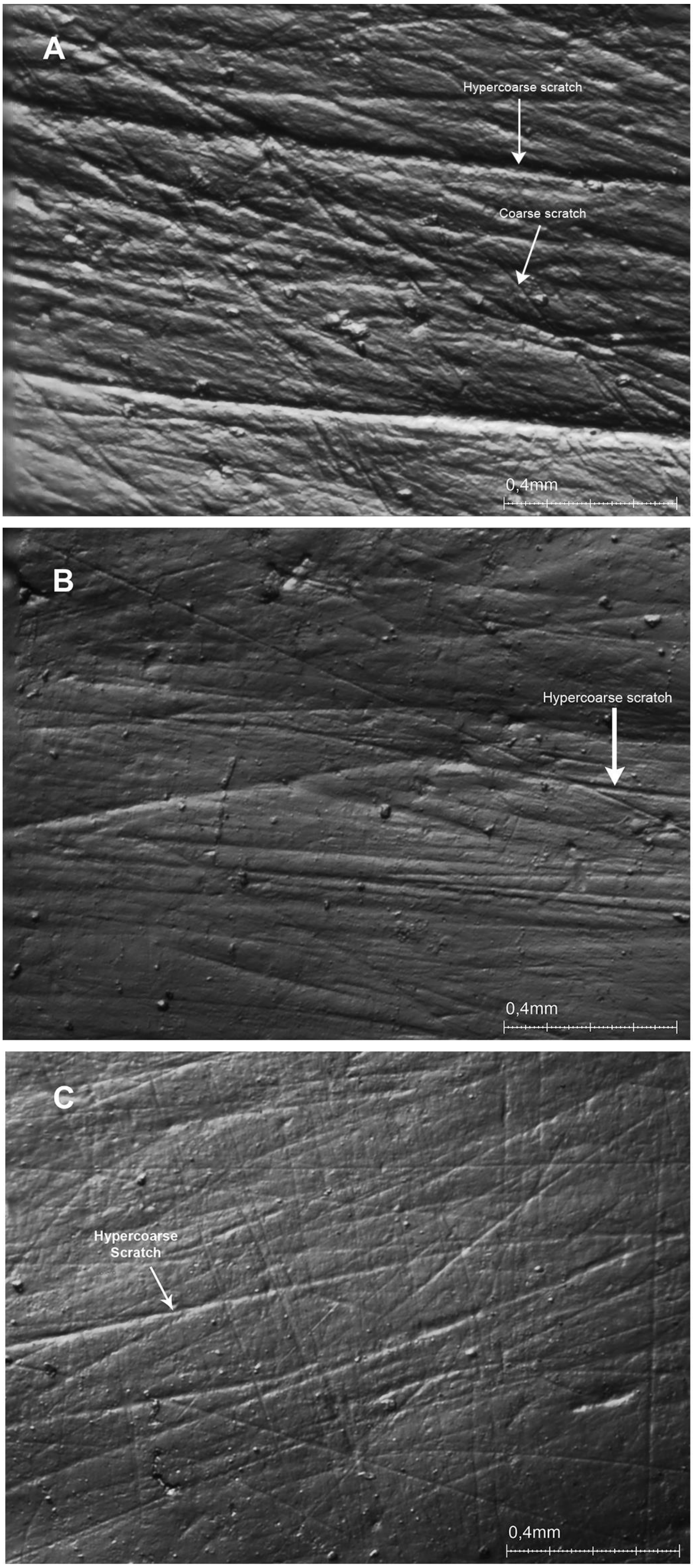
A
Hypercoarse scratch
Coarse scratch
0,4mm
B
Hypercoarse scratch
0,4mm
C
Hypercoarse
Scratch
0,4mm

Figure S3. Photomicrographs of tooth enamel surface from selected Chilean fossil gomphotheres, at 35 times magnification. **A)** Gomphothere from Lagunillas site (SGO.PV.22) (33ºS; North–Central). **B)** Gomphothere from Tagua Tagua site (SGO.PV.47c) (34ºS; North–Central). **C)** Gomphothere from Alto de Boroa site (MRA2462) (38ºS; South–Central).

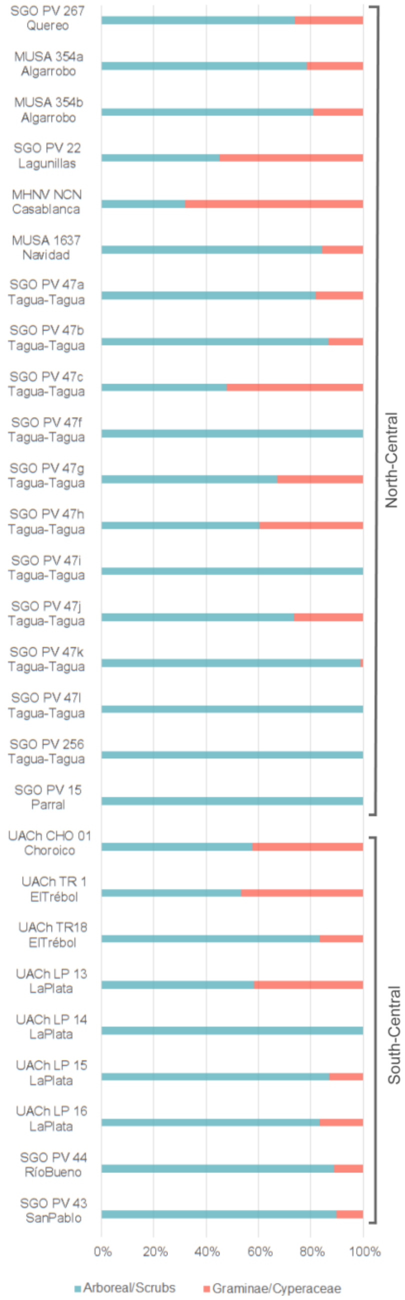

Figure S4. Percentages between arboreal/scrubs elements (light blue) and non-arboreal elements (Graminae/Cyperaceae) (red) based on dental calculus analysis of selected Chilean gomphotheres.

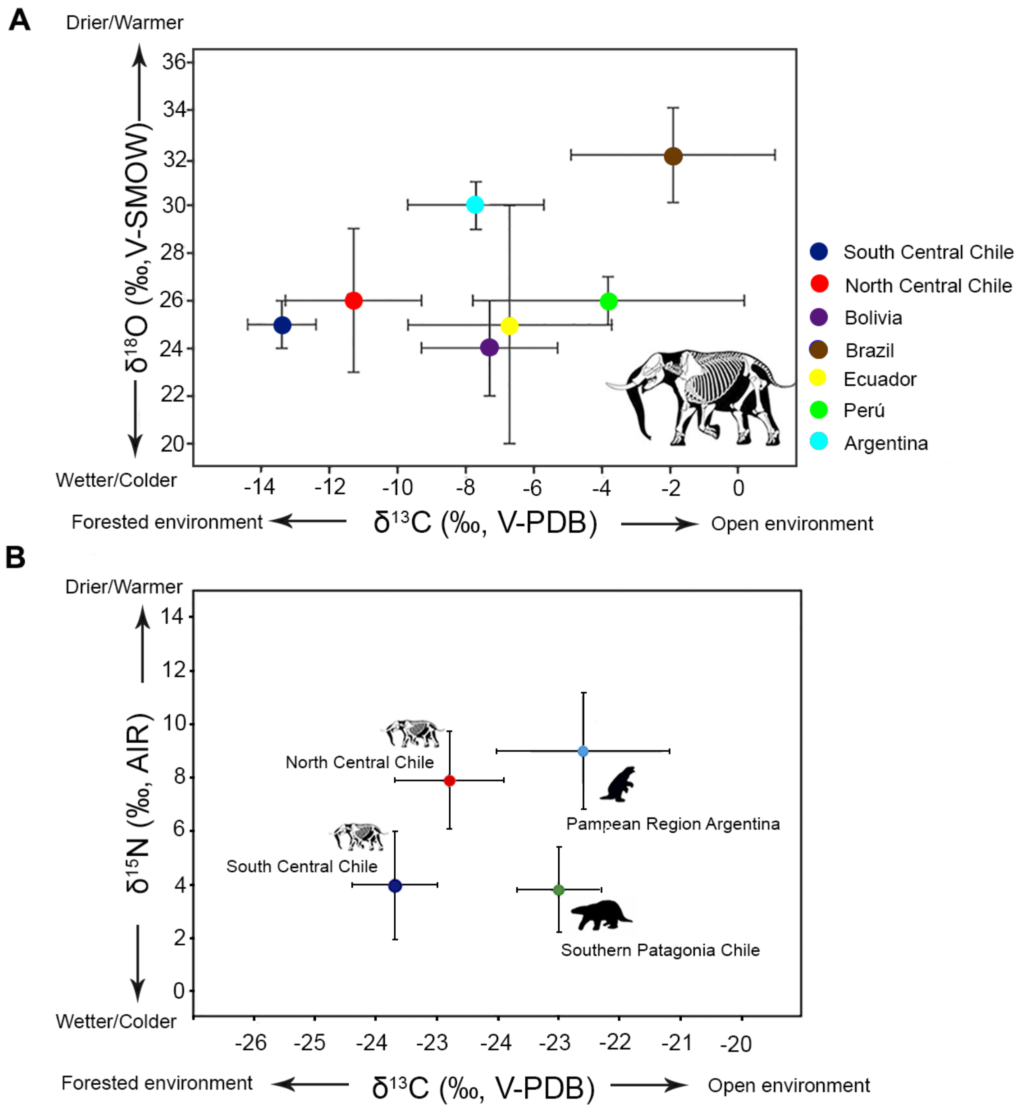

Figure S5. A) Bioapatite mean $\delta^{13}C$ (‰, VPDB) and $\delta^{18}O_{CO3}$ (‰, VSMOW) values ± 1 standard deviation of *Notiomastodon platensis* from Chile. Isotopic results from other contemporaneous sites of South America are shown (24, 36). It is noticeable the low bioapatite $\delta^{13}C$ values depicted by Chilean gomphotheres when compared to specimens (*Notiomastodon platensis* and

Cuvieronius hyodon) from other South America localities. **B**) Collagen mean $\delta^{13}C$ (‰, VPDB) and $\delta^{15}N$ (‰, AIR) values ± 1 standard deviation of gomphotheres from Chile. It is remarkable the latitudinal gradient recorded by collagen $\delta^{15}N$ values between gomphotheres from the North–Central and South-Central areas. Mean $\delta^{13}C$ and $\delta^{15}N$ values of herbivores from the Pampean Region (37) and Southern Patagonia (38) are included in the figure.

Table S1. Summary of stable isotope data and statistical tests. **A**. Bioapatite $\delta^{13}C$ (‰, VPDB) values, **B**. Bioapatite $\delta^{18}O_{CO3}$ (‰, VPDB) values, **C**. Collagen $\delta^{13}C$ (‰, VPDB) values, **D**. Collagen $\delta^{15}N$ (‰, AIR) values. In the case of bioapatite, stable isotope values of our study were analyzed together with values from Sánchez et al. (39), Domingo et al. (24), and González-Guarda et al. (19). In the case of collagen, stable isotope values of our study were analyzed together with values from González-Guarda et al. (19).

A. $\delta^{13}C$ (‰, VPDB)$_{(biopatite)}$					
Area	**n**	**Min**	**Max**	**Mean**	**Standard desviation**
North–Central	38	-14.8	-3.9	-11.3	2.2
South–Central	23	-15.2	-11.7	-13.4	0.8
Mean Rank (North–Central)	**Mean Rank (South–Central)**	**z**	**p-value**		
24.7	6.7	-4.8	0.0001		
B. $\delta^{18}O_{CO3}$ (‰, VPDB)$_{(biopatite)}$					
Area	**n**	**Min**	**Max**	**Mean**	**Standard desviation**
North–Central	38	-12.4	0.6	-4.3	2.5
South–Central	23	-7.1	-2.4	-5.1	0.9

Mean Rank (North–Central)	**Mean Rank (South–Central)**	**z**	**p-value**		
22.4	9	-2.7	0.005		
C. $\delta^{13}C$ (‰, VPDB)$_{collagen}$					
Area	**n**	**Min**	**Max**	**Mean**	**Standard desviation**
North-Central	13	-22.7	-19.2	-21.8	0.9
South-Central	21	-23.9	-21.4	-22.7	0.7
Mean Rank (North–Central)	**Mean Rank (South–Central)**	**z**	**p-value**		
9	8.4	-2.8	0.0045		
D. $\delta^{15}N$ (‰, AIR)$_{collagen}$					
Area	**n**	**Min**	**Max**	**Mean**	**Standard desviation**
North–Central	13	7.1	14.2	7.9	1.8
South–Central	21	1.3	8.5	4	2.1
Mean Rank (North–Central)	**Mean Rank (South–Central)**	**z**	**p-value**		
10.3	7.1	-4.3	0.0001		

Table S2. Summary and statistical tests for the modern equivalent dietary (i.e., vegetation) carbon stable isotope value ($\delta^{13}C_{diet,meq}$) calculated for NC and SC gomphotheres. From bioapatite $\delta^{13}C$ values, modern equivalent vegetation was calculated using the following equation: $\delta^{13}C_{diet,meq} = \delta^{13}C_{leaf} + (\delta^{13}C_{modernatmCO2} - \delta^{13}C_{ancientatmCO2})$, where $\delta^{13}C_{leaf} = \delta^{13}C_{tooth}$ -14.1‰, $\delta^{13}C_{modernatmCO2}$ is -8‰ and $\delta^{13}C_{ancientatmCO2}$ is -6.5‰ (late Pleistocene).

Area	**n**	**Min**	**Max**	**Mean**	**Standard desviation**
North–Central	38	-31	-20	-26.9	2.2
South–Central	24	-31	-27	-29	0.8
Mean Rank (North–Central)	**Mean Rank (South–Central)**	**z**	**p-value**		
24.8	6.6	-5	0.0001		

Table S3. Summary and statistical tests for mean annual temperatures (MATs) calculated for NC and SC areas from gomphothere $\delta^{18}O_{PO4}$ values.

To calculate meteoric water $\delta^{18}O$ values ($\delta^{18}O_{mw}$) from gomphothere tooth enamel $\delta^{18}O_{PO4}$ values, the following equation was used: $\delta^{18}O_{mw\ (VSMOW)}$ = ($\delta^{18}O_{PO4\ (VSMOW)}$ - 23.3)/0.94. Subsequently, MAT was estimated using the linear regression established between MAT and $\delta^{18}O_{mw}$ values: MAT (ºC) = $\delta^{18}O_{mw}$ (VSMOW) +12.68)/0.36 (R^2 = 0.72).

Area	**n**	**Min ºC**	**Max ºC**	**Mean ºC**	**Standard deviation**
North-Central	38	-6	30	18.6	7
South-Central	25	9	23	15.6	2.6
Mean Rank (North–Central)	**Mean Rank (South–Central)**	**z**	**p-value**		
23.2	8.7	-3.5	0.0005		

Table S4. Raw data from stereoscopic microwear analysis for *Notiomastodon platensis* from central Chile. SP = small pits; LP = large pits; FS = fine scratches; CS = coarse scratches. A scratch width score (SWS) was obtained by giving a score of 0 to teeth with predominantly fine (F) scratches per tooth surface, 1 to those with a mixture (Mx) of fine and coarse types of textures, 2 to those with predominantly coarse scratches per tooth surface (C) and a score of 3 to teeth with predominantly hyper-coarse (HC) per tooth surface. HC (ausence/presence) = 0 to ausence; and 1 to presence.

Sample	**Tooth**	**Site/Latitude**	**Number of pits**		**Number of Scratches**		**SWS**				**FS + CS**	**HC (ausence/ presence)**
			SP	LP	FS	CS	F	Mx	C	HC		
SGO.PV. 267	M3	Quereo, 31ºS	18		4	6			2		10	0
SGO.PV. 22	M3	Lagunillas, 33ºS	3			3				3	3	1
SGO.PV. MUSA035 4a	Indet.	Algarrobo, 33ºS	15		8	4		1			12	0
MUSA169 0	M3	Río Rapel, 33ºS	2		6	3		1			9	0
MHNV (ncn)	M2/m2	Casablanca, 33ºS	4		11	3		1			14	1
SGO.PV. 47h	M2/m2	Tagua Tagua, 34ºS	2		5	7			2		12	1
SGO PV.1E	M3	Tagua Tagua, 34ºS	3	12	6	4			2		10	0
SGO PV 47i	M3/m3	Tagua Tagua, 34ºS	4		2	7			2		9	1
SGO.PV. 47a	M3/m3	Tagua Tagua, 34ºS	2			4			2		4	1
SGO.PV. 47b	M3/m3	Tagua Tagua, 34ºS	2		13			1			13	0
SGO.PV. 47j	M3	Tagua Tagua, 34ºS	5		11	1		1			12	0
SGO.PV. 13a	M3	Tagua Tagua, 34ºS	3		7	6			2		13	1
SGO.PV. 47c	M3/m3	Tagua Tagua, 34ºS	6		17	2		1			19	1

SGO.PV. 46a	M3/m3	Tagua Tagua, 34ºS	5		13	3		1			16	1
SGO.PV. 46b	M3/m3	Tagua Tagua, 34ºS	2		5	5		1			10	1
SGO.PV. 47f	M3/m3	Tagua Tagua, 34ºS	3		4	5			2		9	1
SGO.PV. 47k	M2/m2	Tagua Tagua, 34ºS	4		3	4			2		7	1
SGO.PV. 48a	M1/m1	Tagua Tagua, 34ºS	3			10			2		10	0
SGO.PV. 256	M3/m3	Tagua Tagua, 34ºS	5		6	5			2		11	1
SGO.PV. 47l	M3/m3	Tagua Tagua, 34ºS	2	17	1	4			2		5	1
SGO.PV. 55	M3/m3	Parral, 36ºS	3		9	3			2		12	1
SGO.PV. 15a	M3/m3	Parral, 36ºS	2	4		4			2		4	1
SGO.PV. 15b	M3/m3	Parral, 36ºS	3		4	2			2		6	0
MRA2462	M3	Alto de Boroa, 38ºS	2		8	4			2		12	1
MRA2461	M3	Alto de Boroa, 38ºS	3		7	5			2		12	1
UACh PV MA 1	m2	Máfil, 39ºS	4	6		4			2		4	1
UACh PV LP 13	m2	La Plata, 40ºS	2	7	3	6			2		9	0
MHMOP/ MU/3B	Indet.	Mulpulmo, 40ºS	3	9	4	5			2		9	1
MHMOP/ MU/5	M2/m2	Mulpulmo, 40ºS	3		6	8			2		14	1
MHMOPI/ 628	M2	Pilauco, 40ºS	3		4	5			2		9	1
MHMOPI/ 627	M2	Pilauco, 40ºS	4		4	5			2		9	1
UACh PV FR 22	Indet.	Frutillar, 41ºS	4		1	3				3	4	1
MHAMM A02156	m3	Monte Verde, 41ºS	2	3		6			2		6	1
MMC 5	M3	Castro, 42ºS	5		4	4			2		8	1
MMC 6	m3	Castro, 42ºS	15		3	3			2		6	1

Institutions: SGO.PV, Museo Nacional de Historia Natural; MRA, Museo Regional de la Araucanía; UACh PV, Universidad Austral de Chile Paleontología de Vertebrados; MHMO, Museo Histórico Municipal de Osorno; MMC, Museo Municipal de Castro; MUSA, Museo de

Historia Natural de Valparaíso; MHAMM, Museo Histórico y Antropológico Mauricio Van de Maele.

Tabla S5. Microwear results for fossil gomphotheres grouped latitudinally. Abbreviations: TNL = total number of localities; N = sample size; Np= average number of pits; SDNp = standard deviation of the average number of pits; Ns = average number of scratches; SDNs = standard deviation of the average number of scratches; %LP = percentage of individuals with large pits; SWS = scratch width score; %HC = percentage of individuals with hypercoarse scratches; %0–17 = percentage of individuals with low numbers of scratches (from 0 to 17 scratches per counting area).

Latitude	TNL	N	Np	SDNp	Ns	SDNs	%LP	SWS	%HC	%0-17
31°–36°S (North–Central)	7	23	4.3	4	10	4	14	1.8	68	95
38°–42°S (South–Central)	8	12	4.1	3.5	8.5	3	33	2	92	100

Table S6. Percentages of arboreal/scrubs/herbs phytoliths; Number of diatoms/sponge spicules; Microfossils concentration.

Localities and latitude	Sample	Tooth	% Arboreal	% Scrubs	% Herbs	% Cyperacea	Nº Diatoms/spicules
Quereo, 31ºS	SGO PV 267	m3	96.6		3.4	0	0
Illapel, 31ºS	SGO PV 40	M2	100		0	0	1
Lagunillas, 33ºS	SGO PV 22	M3	45	0	41	14	3
Algarrobo, 33ºS	MUSA354a	Indet.	75.5	3	21	0	1
Algarrobo, 33ºS	MUSA354b	Indet.	76	5	19	0	0
Navidad. 33ºS	MUSA1637	M3/m3	84	0	16	0	0
Casablanca, 33ºS	MNHV (ncn)	M2/m2	25	7	68	0	107

Tagua – Tagua, 34ºS	SGO PV 47a	M3	81.8		16.8	1.4	4
	SGO PV 47b	M3/m3	67.6	20	13.4	0	2
	SGO PV 47c	M3/m3	26	22	32	20	240
	SGO PV 47f	M3/m3	100		0	0	0
	SGO PV 47g	M3/m3	67.7		33.3	0	0
	SGO PV 47h	M2/m2	92.6	0.22	6.2	0	0
	SGO PV 47i	M3/m3	100		0	0	0
	SGO PV 47j	M3	73.5		24.5	2.5	28
	SGO PV 47k	M2/m2	90.7	1.33	8	0	14
	SGO PV 47l	M3/m3	98.4	1.6	0	0	0
	SGO PV 256	M3/m3	100		0	0	0
Parral, 36ºS	SGO PV 15a	M3/m3	80.9	4.8	14.3	0	0
El Trébol, 39ºS	UACh PV TR 1	m3	48.7	4.7	46.6	0	0
	UACh PV TR 18	m3	82.6		17.4	0	0
Choroico, 40ºS	UAChPVCHO01	M3	53	4.1	42.1	0	2
San Pablo de Tramalhue, 40ºS	SGO PV 43	M3	86.2	3.6	10.2	0	1
La Plata, Futrono, 40ºS	UACh PV LP 13	m2	79.9	13.4	6.7	0	0
	UACh PV LP 14	m2	63.3	36.7	0	0	0
	UACh PV LP 15	m2	84.8	2.2	13	0	0
	UACh PV LP 16	m2	83.4		16.6	0	0
Rio Bueno, 40ºS	SGO PV 44	M3	83.2	5.8	11	0	0

Table S7. Radiocarbon dates on Gomphotheriidae obtained from bone collagen and using AMS. All dates have been calibrated to calendar years using the software Calib 7.0.4 and the Southern Hemisphere calibration curve SH13. Two different pretreatments of bone collagen were used: [a] XAD, [b] Ultrafiltration.

Taxon	Collection number	Locality	^{14}C Lab number	Anatomical Element	^{14}C age	Cal mean (cal yr BP)	Cal 2σ range (cal yr BP)	Reference
Notiomastodon platensis	SGO.PV.267	Quereo	CAMS 175732 [a]	Molar root, collagen	10970 ± 70	12799	12703-12982	This study
Notiomastodon platensis	SGO.PV.256	Tagua Tagua	PSUAMS 2429 [a]	Molar root, collagen	11750 ± 60	13527	13424-13717	This study
Notiomastodon platensis	SGO.PV.47k	Tagua Tagua	CAMS 175743 [a]	Molar root, collagen	12260 ± 80	14123	13805-14524	This study
Notiomastodon platensis	MRA2462	Alto de Boroa	PSUAMS 2430 [a]	Molar root, collagen	11875 ± 50	13655	13545-13770	This study
Notiomastodon platensis	UACh PV MA 1	Máfil	CAMS 175749 [a]	Molar root, collagen	11790 ± 80	13575	13434-13751	Gonzalez-Guarda et al., 2017
Notiomastodon platensis	GEOUACh/P/80	El Trébol	UCI 101833 [b]	Molar root	28760 ± 390	32752	31657-33661	Gonzalez-Guarda et al., 2017
Notiomastodon platensis	UACh PV CHA 01	Chan Chan	PSUAMS 2423 [a]	Molar, collagen	10250 ± 45	11890	11745-12050	This study
Notiomastodon platensis	UACh PV CHO 01	Choroico	PSUAMS 2422 [a]	Molar, collagen	11345 ± 45	13154	13070-13264	This study
Notiomastodon platensis	GEOUACh 81	La Plata	UCI 102088 [b]	Molar root	12315 ± 40	14185	14021-14463	Gonzalez-Guarda et al., 2017
Notiomastodon platensis	SGO.PV.44	Rio Bueno	CAMS 175733 [a]	Molar root, collagen	11090 ± 70	12910	12747-13062	Gonzalez-Guarda et al., 2017

Notiomastodon platensis	SGO.PV.43	San Pablo	CAMS 175744 [a]	Molar root, collagen	11380 ± 70	13188	13064-13317	Gonzalez-Guarda et al., 2017
Notiomastodon platensis	indet.	Mulpulmo	PSUAMS 2425 [a]	Molar, collagen	19550 ± 130	23499	19550-23086	This study
Notiomastodon platensis	indet.	Nochaco	PSUAMS 2424 [a]	Molar root, collagen	17130 ± 90	20612	17130-20339	This study
Notiomastodon platensis	MHMOPI/628	Pilauco	PSUAMS 2415 [a]	Molar root, collagen	13240 ± 60	15861	13240-15644	This study
Notiomastodon platensis	GEOUACH 132	Los Notros	AA 109501	Tusk	13,585± 81	16,310	16,048-16,614	This study
Notiomastodon platensis	MMC 5	Castro, Chiloé	PSUAMS 2426 [a]	Molar root, collagen	13270 ± 60	15900	13270-15685	This study

Institutions: SGO.PV, Museo Nacional de Historia Natural; MRA, Museo Regional de la Araucanía; UACh PV, Universidad Austral de Chile, Paleontología de Vertebrados; MHMO, Museo Histórico Municipal de Osorno; MMC, Museo Municipal de Castro; GEOUACH, Geología Universidad Austral de Chile; CAMS, center for accelerator mass spectrometry in Lawrence Livermore National laboratories, California; PSUAMS, Human Paleoecology and Isotope Geochemistry Lab of the Pennsylvania State University; UCI, Keck Carbon Cycle AMS Facility, Earth System Science Dept, Univ. California – Irvine; AA, NSF Arizona AMS Laboratory.

References

1. Berman A-L, Silvestri G-E, Tonello M-S (2016) Differences between Last Glacial Maximum and present-day temperature and precipitation in southern South America. *Quat Sci Rev* 150, 221–233.

2. Moreno P, et al. (2015). Radiocarbon chronology of the last glacial maximum and its termination in northwestern Patagonia. *Quat Sci Rev* 122, 233–249.

3. Mathiasen P, Premoli, A-C (2010) Out in the cold: genetic variation of *Nothofagus pumilio* (Nothofagaceae) provides evidence for latitudinally distinct evolutionary histories in austral South America. *Mol Ecol* 19(2): 371–385.

4. Lamy F, et al. (2007) Modulation of the bipolar seesaw in the southeast Pacific during termination 1. *Earth Planet Sci Lett* 259, 400–413.

5. Valero-Garcés, B-L et al. (2005). Palaeohydrology of Laguna de Tagua Tagua (34°30’ S) and Moisture Fluctuations in Central Chile for the Last 46,000 yr, *J Quat Sci* 20 (7-8), 625–641.

6. Kaiser J, Schefuß E, Lamy F, Mohtadi M, Hebbeln D (2008) Glacial to Holocene changes in sea surface temperature and coastal vegetation in north central Chile: high versus low latitude forcing. *Quat Sci Rev* 27(21): 2064–2075.

7. Iacumin P, Bocherens H, Mariotti A, Mariotti A, Longinelli A (1996) Oxygen isotope analyses of coexisting carbonate and phosphate in biogenic apatite: a way to monitor diagenetic alteration of bone phosphate? *Earth Planet Sci Lett* 142, 1–6.

8. Clementz M-T, Fox-Dobbs K, Wheatley P-V, Koch, P-L, Doak D-F (2009) Revisiting old bones: coupled carbon isotope analysis of bioapatite and collagen as an ecological and palaeoecological tool. *Geol J* 44(5): 605–620.

9. Ambrose S-H, (1990). Preparation and characterization of bone and tooth collagen for isotopic analysis. *J Archaeol Sci* 17, 431–451.

10. Solounias N, Semprebon G (2002) Advances in the reconstruction of ungulate ecomorphology with application to early fossil equids. *Am Mus Novit* 1–49.

11. Semprebon G-M, Rivals F, Solounias N, Hulbert R-C (2016) Paleodietary reconstruction of fossil horses from the Eocene through Pleistocene of North America. *Palaeogeogr Palaeoclimatol Palaeoecol* 442, 110–127.

12. Alvin K-L, Fraser C-J, Spicer R-A (1981) Anatomy and palaeoecology of *Pseudofrenelopsis* and associated conifers in the English Wealden. *Paleontology* 24, 759–778.

13. Grine F-E, 1986. Dental evidence for dietary differences in *Australopithecus* and *Paranthropus*: a quantitative analysis of permanent molar microwear. *J. Hum Evol* 15, 783–822.

14. Cordova C-E, Avery G (2017) African savanna elephants and their vegetation associations in the Cape Region, South Africa: Opal phytoliths from dental calculus on prehistoric, historic and reserve elephants. *Quat Int* 443: 189–211.

15. Weyrich L-S, et al. (2017) Neanderthal behaviour, diet, and disease inferred from ancient DNA in dental calculus. *Nature* 544, 357–361.

16. Power R-C, et al. (2015) Dental calculus evidence of Taï Forest Chimpanzee plant consumption and life history transitions Scientific Reports, *Sci Rep* 5, 15161.

17. Weber S, Price M (2016) What the pig ate: A microbotanical study of pig dental calculus from 10th–3rd millennium BC northern Mesopotamia, *J Archaeol Sci* 6, 819–827.

18. Tornero C, et al. (2013) Seasonality and season of birth in early Eneolithic sheep from Cheia (Romania): methodological advances and implications for animal economy. *J Archaeol Sci* 40, 4039–4055.

19. González-Guarda E, et al. (2017) Late Pleistocene ecological, environmental and climatic reconstruction based on megafauna stable isotopes from northwestern Chilean Patagonia. *Quat Sci Rev* 170, 188–202.

20. Longin R (1971) New method of collagen extraction for radiocarbon dating. *Nature* 230(5291): 241–242.

21. Bocherens H, et al. (1991). Biogéochimie isotopique (^{13}C, ^{15}N, ^{18}O) et paléoécologie des ours pléistocènes de la grotte d'Aldène. *Bull Mus Anthropol Prehist* Monaco, 34: 29–49.

22. Tipple B-J, Meyers S-R, Pagani M (2010) Carbon isotope ratio of cenozoic CO_2: a comparative evaluation of available geochemical proxies. *Paleoceanography* 25(3).

23. Cerling T-E, Harris J-M (1999) Carbon isotope fractionation between diet and bioapatite in ungulate mammals and implications for ecological and paleoecological studies. *Oecologia* 120(3): 347–363.

24. Domingo L, Prado J-L, Alberdi M-T (2012) The effect of paleoecology and paleobiogeography on stable isotopes of Quaternary mammals from South America. *Quat Sci Rev* 55, 103–113.

25. Ayliffe L-K, Lister A-M, Chivas A-R (1992) The preservation of glacial interglacial climatic signatures in the oxygen isotopes of elephant skeletal phosphate. *Palaeogeogr Palaeoclimatol Palaeoecol* 99, 179–191.

26. Rozanski K, Araguas-Araguas L, Gonfiantini R, (1993) Isotopic patterns in modern global precipitation. In: Swart, P.K., Lohmann, K.C., McKenzie, J., Savin, S. (Eds.), *Climate Change in Continental Isotopic Records* 78, pp 1–36. *Geophys Monogr Ser*.

27. Kohn M-J, (2010) Carbon isotope compositions of terrestrial C_3 plants as indicators of paleoecology and paleoclimate. *Proc Natl Acad Sci USA* 107(46): 19691–19695.

28. Asevedo L, Winck G-R, Mothé D, Avilla L-S (2012) Ancient diet of the Pleistocene gomphothere *Notiomastodon platensis* (Mammalia, Proboscidea,

Gomphotheriidae) from lowland mid-latitudes of South America: Stereomicrowear and tooth calculus analyses combined. *Quat Int* 255, 42–52.

29. Rivals F, Solounias N, Mihlbachler M-C (2007) Evidence for geographic variation in the diets of late Pleistocene and early Holocene *Bison* in North America, and differences from the diets of recent *Bison*. *Quat Res* 68, 338–346.

30. Wesolowski V., Souza, S.M.F.M., de, Reinhard, K.J., Ceccantinni, G., 2007. Grânulos de amido e tólitos em cálculos dentários humanos: contribuiçaõ ao estudo do modo de vida e subsistência de grupos sambaquianos do litoral sul do Brasil. *Rev Museu Arqueol Etnol* (Saõ Paulo) 17, 191–210.

31. Maher L-J (1981) Statistics for microfossil concentration measurements employing samples spiked with marker grains. *Rev Palaeobot Palynol* 32, 153-191.

32. Wesolowski V, de Souza S-M-F-M, Reinhard K-J, Ceccantini G (2010) Evaluating microfossil content of dental calculus from Brazilian sambaquis. *J Archaeol Sci* 37(6): 1326–1338.

33. Stafford T-W, Brendel K, Duhamel R-C (1988) Radiocarbon, ^{13}C and ^{15}N analysis of fossil bone: removal of humates with XAD-2 resin. *Geochim Cosmochim Acta*, 52(9): 2257–2267.

34. Stuiver M, Reimer P (1986–2014) Calib Radiocarbon Calibration Program.

35. Luebert F, Pliscoff P (2006) *Sinopsis bioclimática y vegetacional de Chile*. Editorial Universitaria.

36. Dantas M, et al. (2017) Isotopic paleoecology of the Pleistocene megamammals from the Brazilian Intertropical Region: Feeding ecology ($\delta^{13}C$), niche breadth and overlap. *Quat Sci Rev* 170, 152–163.

37. Bocherens H, et al. (2016). Paleobiology of sabretooth cat *Smilodon populator* in the Pampean Region (Buenos Aires Province, Argentina) around the Last Glacial Maximum: Insights from carbon and nitrogen stable isotopes in bone collagen. *Palaeogeogr Palaeoclimatol Palaeoecol* 449, 463–474.

38. Prevosti F-J, Martin F-M (2013) Paleoecology of the mammalian predator guild of Southern Patagonia during the latest Pleistocene: ecomorphology, stable isotopes, and taphonomy. *Quat Int* 305 74–84.

39. Sánchez B, Prado J-L, Alberdi M-T (2004) Feeding ecology, dispersal, and extinction of South American Pleistocene gomphotheres (Gomphotheriidae, Proboscidea). *Paleobiology* 30, 146–161.